Supplementary Text: Methods

Protein expression and purification

Unlabeled wild-type dSP-AVR1-CO39 lacking the signal peptide (residues Trp 23 to Cys 89) and RGA5_S (residues Leu 982 to Met 1116) were expressed and purified as previously described (1). DNAs coding for dSP-AVR1-CO39 mutants were chemically synthesized with codons optimized for *Escherichia coli* (Life Technologies) and inserted into the pET-28a expression vector as previously described for dSP-AVR1-CO39 wild-type (1). The sequences of these constructs were verified by DNA sequencing. Expression and purification strategies were identical to that of wild-type dSP-AVR1-CO39 (1). Briefly, the recombinant vectors were expressed in *E. coli* strain BL21 (DE3). Cells were lysed by sonication in 20 mM Tris-HCl pH 8.0, 500 mM NaCl and the soluble proteins were separated by centrifugation. Proteins were purified with Ni-Chelating Sepharose^{TM} Fast Flow Agarose, followed by Superdex^{TM} 75 10/300 GL gel-filtration chromatography (GE Healthcare). The peak fractions were pooled and concentrated to 4-12 mg mL^{-1} with an Amicon Ultra-15 centrifugal filter with a 5-kDa molecular weight cut-off value (Millipore).

For NMR and investigation of dSP-AVR1-CO39/RGA5$_{HMA}$ complex formation by ITC, dSP-AVR1-CO39 wild-type and mutants and RGA5$_{HMA}$ were prepared as previously described (2, 3). Uniform ^{15}N labeling of recombinant proteins for NMR was obtained by growing *E.coli* in C-750501 media (4) containing $^{15}NH_4Cl$ as the sole nitrogen source. After purification, the fractions containing the pure protein were evaluated by SDS-PAGE and stored at -20°C until analysis.

Crystallization

RGA5_S and the RGA5_S/AVR1-CO39 complex were crystallized by the sitting-drop diffusion method at 16 ℃ using an Oryx4 robot (Douglas Instrument, United Kingdom) in MRC 96-well MRC plates (XtalQuest Ltd) as described (1).

RGA5_S was concentrated to 6.4 mg mL^{-1} in 20 mM NaH_2PO_4/Na_2HPO_4 pH 7.0, 150

mM NaCl, 4 mM dithiothreitol (DTT), and 4 mM ethylenediaminetetraacetic acid (EDTA). Small crystals of RGA5_S were produced after 3 days in 0.2 M ammonium nitrate and 20% (w/v) PEG 3350. The reservoir solutions were optimized over ammonium nitrate range 0.18 to 0.22 M in one dimension and a 18% to 22% (w/v) PEG 3350 concentration gradient in the second dimension using 96-well MRC plates (XtalQuest Ltd). After optimization, the crystal with the highest quality was obtained from 0.18 M ammonium nitrate and 20% (w/v) PEG 3350 within one week.

RGA5_S and dSP-AVR1-CO39 were mixed at a 1:1 molar ratio and were crystallized. Crystals with high quality were obtained after 2-3 weeks with reservoir solution containing 0.1 M sodium acetate-HCl pH 4.6, 1.1 M ammonium tartrate dibasic (1).

X-ray data collection, structure determination and refinement

Prior to data collection, crystals were first transferred into mother liquor with an additional 20% glycerol as cryo-protectant, mounted in a loop and immediately flashed-cooled in liquid nitrogen for later use. Diffraction data were collected at the Shanghai Synchrotron Research Facility (SSRF, China) .

Diffraction data were indexed and scaled with xia2 implemented in the CCP4 suite (5, 6). The structures were solved using molecular replacement (MR) method with *Phaser* (7). For the RGA5_S structure, a homologous structure of a copper binding domain from HMA7 (PDB code: 3DXS) was used as a search model. The structure of the RGA5_S/dSP-AVR1-CO39 complex was solved using the apo structure of RGA5_S determined in the present study and the structure of AVR1-CO39 (PDB: 2MYV). In both cases, models were subsequently improved through iterative cycles of manual rebuilding and refinement using COOT (8) and PHENIX with TLS (Translation/Libration/Screw) restraints (7). The refinement statistics and model quality parameters are detailed in Table S1.

Stereochemical validation of the model was performed with MolProbity (9). Atomic coordinates and structure factors of RGA5_S and RGA5_S/dSP-AVR1-CO39

complexes were deposited in the PDB with the accession codes 5ZNE and 5ZNG, respectively. Figures containing structures were generated with PyMOL (PyMOL Molecular Graphics system, Version 1.6 Schrodinger, LLC).

Circular dichroism (CD) spectroscopy

CD spectral analysis was performed on a Chirascan-plus spectropolarimeter (Applied Photophysics, Leatherhead, UK) to estimate the protein secondary structure. Proteins were prepared as described for crystallography in 20 mM Tris-HCl pH 8.0 and 100 mM NaCl, with the final concentration of 0.1- 0.2 mg mL^{-1}. Using a quartz cell with a 1 mm path length at room temperature, spectra were recorded from 200 nm to 260 nm at a scan speed of 60 nm min^{-1} for the corresponding buffer of each sample.

Nuclear magnetic resonance spectroscopy

Spectra were acquired on 800 and 700 MHz Avance Bruker spectrometers equipped with triple-resonance (^{1}H, ^{15}N, ^{13}C) z-gradient cryo-probe at 305 K. Experiments were recorded using the TOPSPIN pulse sequence library (v. 2.1). All spectra are referenced to the internal reference DSS (4,4-dimethyl-4-silapentane-1-sulfonic acid) for the ^{1}H dimension and indirectly referenced for the ^{15}N dimensions (10). Spectra were processed using Topspin (v. 3.2) and were analyzed using strip-plots with Cindy in house software and CCPN analysis (v. 2.4.2) (11). For dSP-AVR1-CO39^{T41V} and dSP-AVR1-CO39$^{W23A/K24A/T41G}$ mutants, side chain assignments were carried out using ^{15}N-NOESY-HSQC and ^{15}N-TOCSY-HSQC 3D spectra.

NMR experiments

For the assignments, ^{15}N-labeled dSP-AVR1-CO39^{T41V} and dSP-AVR1-CO39$^{W23A/K42A/T41G}$ (1 mM) in 20 mM sodium phosphate, pH 6.8, 150 mM NaCl and 1 mM DTT were used. For the titrations of ^{15}N-labeled dSP-AVR1-CO39, different samples with constant concentrations of dSP-AVR1-CO39 (50 µM) and various concentrations of unlabeled $RGA5_{HMA}$ (ratios 2:1, 1:1, 0.5:1, 0.25:1, 0:1 for the reference) were prepared. HSQC spectra were recorded at 305 K on a Bruker Avance

700 MHz spectrometer. Chemical shift differences were measured from the HSQC spectra of dSP-AVR1-CO39 alone and the effector/HMA complex at R=2. They are reported as Hamming distance weighted by the magnetogyric ratios (12). All the NMR samples were prepared with addition of 10% D_2O and 1 μM DSS as a reference.

Analytical gel filtration

The complex formation between RGA5_S with wild-type or mutants of dSP-AVR1-CO39 was examined by analytical gel size exclusion chromatography using Superdex^{TM} 75 10/300 GL gel-filtration chromatography (GE Healthcare). The column was pre-equilibrated with a gel filtration buffer (20 mM Tris-HCl pH 8.0, 150 mM NaCl, 5 mM DTT, 4 mM EDTA). Samples of individual proteins (250 μL at 1100 μM each) or the mixtures (250 μL at 1100 μM each) were loaded to Superdex^{TM} 75 column and then eluted at a flow rate of 0.7 mL min^{-1}. Fractions of 1 mL each were collected and subjected to SDS-PAGE analysis followed by Coomassie blue staining.

Isothermal titration calorimetry (ITC)

Isothermal titration calorimetry (ITC) experiments with RGA5_S were carried out on a iTC200 isothermal titration calorimeter at 25 °C (Malvern Instruments Ltd). The experimental parameter setting and the calculation of equilibrium dissociation constant (*Kd*) were identical to previous description (1).

Experiments with $RGA5_{HMA}$ were performed on a VP-ITC instrument (Microcal, Northampton, USA). The protein samples were buffer exchanged using dialysis at 4 °C into the ITC buffer (20 mM Tris, pH 8.5, 150 mM NaCl and 2 mM β-mercaptoethanol) to minimize undesirable buffer-related effects. The dialysis buffer was used in all preliminary equilibration and washing steps. Protein concentrations were measured using a NanoDrop 2000 spectrometer and BCA Kit assays (Pierce). The $RGA5_{HMA}$ sample was used in the binding reactions. Titration of $RGA5_{HMA}$ (80 μM) in the cell (2 mL) was performed by sequential addition of dSP-AVR1-CO39 (at 1 mM; 22 injections of 10 μL). Data were analyzed by a single site model using the Origin

Software.

Analytical ultracentrifugation

Sedimentation velocity analytical ultracentrifugation (SV-AUC) was performed in a Beckman Coulter XLI analytical ultra-centrifuge. The individual proteins at 1mg mL^{-1} were dissolved in 20 mM Tris-HCl pH 8.0, 150 mM NaCl. The RGA5_S/dSP-AVR1-CO39 complex was prepared at a 1:1 ratio and incubated on ice for at least 3 h prior to loading. Samples were centrifuged in an An-50Ti rotor at 40000 rpm at 20 ˚C. The data were collected using interference optics and the related sedimentation coefficient distributions *c*(*s*) were calculated using the program SEDEIT (13).

Growth of plants and fungi and infection assays

Rice plants (*Oryza sativa* L.) were grown as described (14). *Nicotiana benthamiana* plants were grown in a growth chamber at 22 °C with a 16 hours light period. *M. oryzae* isolates and transgenic strains were grown as described (15). For the determination of interaction phenotypes and gene expression, a suspension of fungal conidiospores (30000 spores.ml^{-1}) was spray-inoculated on the leaves of 3-week-old rice plants. Rice leaves were collected and scanned 7 days after inoculation.

Constructs for yeast two-hybrid, Co-IP and *M. oryzae* transformation

PCR products used for cloning were generated using Phusion High-Fidelity DNA Polymerase (Thermo Fisher) using primers listed in Table S2. Details of constructs are given in Table S3.

Briefly, all ENTRY vectors used for LR cloning were obtained either by Gateway BP cloning (Life Technologies) into the pDONR207 vector or through site-directed mutagenesis (Quikchange Lightning Technology, Agilent Technologies) using an ENTRY clone as template. Plasmids used for yeast two-hybrid or Co-IP were generated by Gateway LR cloning (Life Technologies) using the ENTRY vectors described above and appropriate destination vectors listed in Table S3.

Plasmids used for *M. oryzae* transformation were created by site-directed mutagenesis (Quikchange Lightning Technology, Agilent Technologies) to introduce point mutations in the sequence of AVR1-CO39.

All constructs were verified by sequencing of the insert and the flanking sequences.

Yeast two-hybrid analysis

Yeast two-hybrid tests were performed as described (15) using the Matchmaker Gold Yeast Two-Hybrid system (Clontech).

Transient protein expression in *N. benthamiana*

Agro-infiltration in *N. benthamiana* were performed as described (15).

Protein extraction immunoblot and co-immunoprecipitation

Protein extraction from *N. benthamiana* leaves and co-IP experiments were performed as described in (15) with the following modification: magnetic GFP-trap_M beads were replaced by magnetic GFP-trap_MA (Chromotek). Total yeast protein was extracted as described (16). For immunoblotting analysis, proteins were separated by SDS-PAGE using precast NuPAGE gels (Life Technologies) and transferred to a nitrocellulose membrane (iBlot 2 transfer stacks, Life Technologies). Membranes were blocked in 5% skimmed milk and probed with anti-HA (Roche anti-HA-HRP 3F10), anti-Myc mouse monoclonal antibodies (Roche) or anti-GFP mouse antibodies (Roche) followed, if required, by goat anti-mouse antibodies conjugated with horseradish peroxidase (Sigma). Labeling was detected using the Immobilon western kit (Millipore). Membranes were stained with Ponceau S to confirm equal loading.

RNA extraction and qRT-PCR analysis

RNA was extracted from infected rice leaves of the highly blast susceptible temperate japonica rice variety Maratelli with TRIZOL reagent (Invitrogen). Reverse transcription was performed with oligo(dT)18 primers and quantitative PCR was performed using LC 480 SYBR Green I Master mix (Roche) and a Lighcycler 480 instrument (Roche)

with the primers indicated in Table S2 and the following conditions: 95 °C for 10 min; 40 cycles of 95 °C for 15 s, 60 °C for 20s and 72 °C for 30 s; then 95 °C for 5 min and 40 °C for 30 s. Data were analyzed using the ΔΔCt method applying the formula $2^{-\Delta CT}$, where ΔCT is the difference in threshold cycle (CT) between the gene of interest and *Actin* (*MGG_03982*) used as a constitutively expressed reference gene. For each isolate, four biological replicate samples were analyzed.

Statistical analysis for pathogenicity tests

For each *M. oryzae* strain tested, lesion areas were measured on 10 leaves from 10 independent rice plants using ImageJ (https://imagej.nih.gov/ij/). To determine whether lesion areas induced by the different AVR1-CO39 mutants on rice are significantly different, a log-transformation was applied to the data prior to an ANOVA with mutant and strains within mutant as factors followed by a Tukey HSD test applied to the mutants.

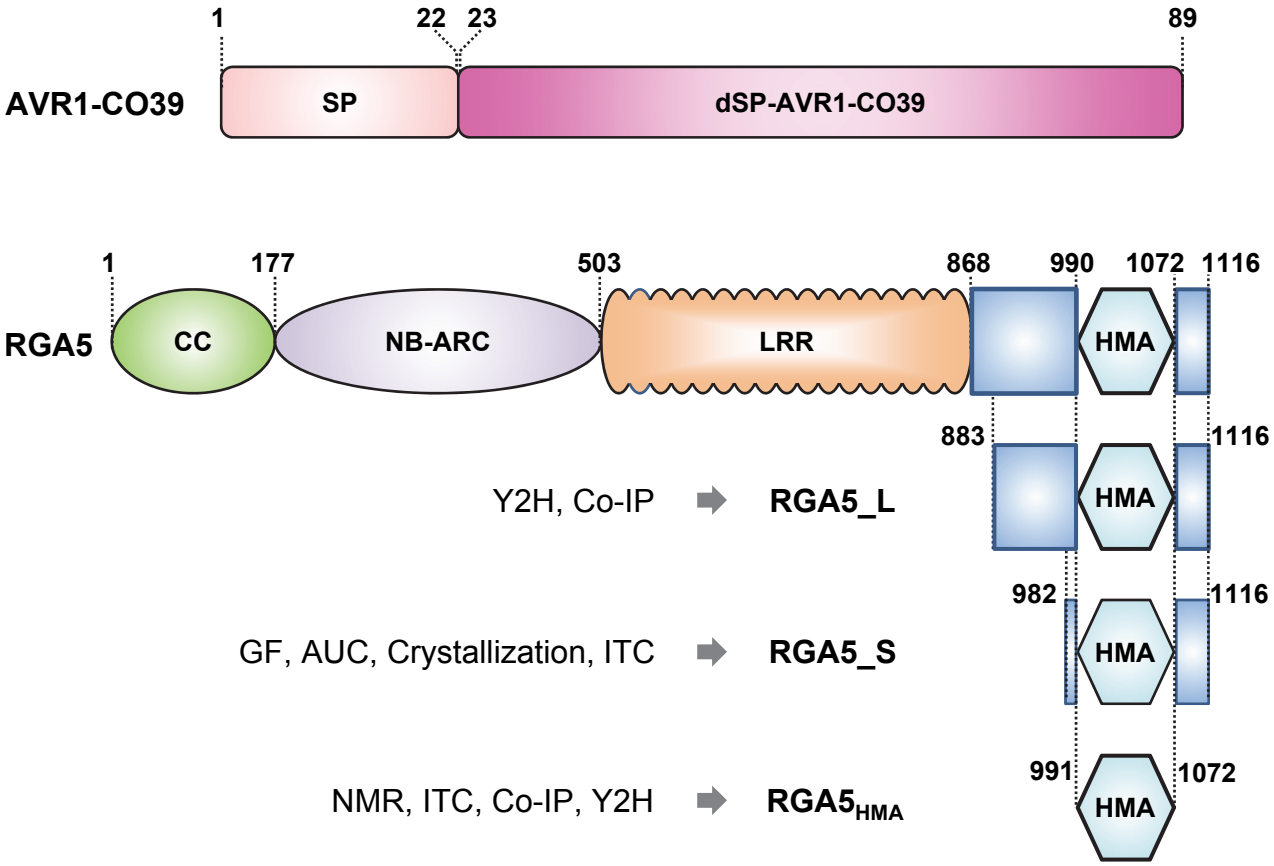

Supplemental Figure 1: Schematic representations of the AVR1-CO39 protein and the different RGA5 constructs used in this study. The mature effector domain is shown in magenta (dSP-AVR1-CO39) and the signal peptide (SP) in blue (amino acids positions are indicated). CC: Coiled Coil, HMA: Heavy Metal Associated domain, NB-ARC: Nucleotide-binding Apaf-1, R-protein, CED4-shared domain, LRR: Leucine Rich Repeat domain. Fragment boundaries are indicated. Y2H: Yeast Two-Hybrid, Co-IP: Co-Immunoprecipitation, GF: Gel Filtration, AUC: Analytical Ultracentrifugation, ITC: Isothermal Titration Calorimetry, NMR: Nuclear Magnetic Resonance spectroscopy.

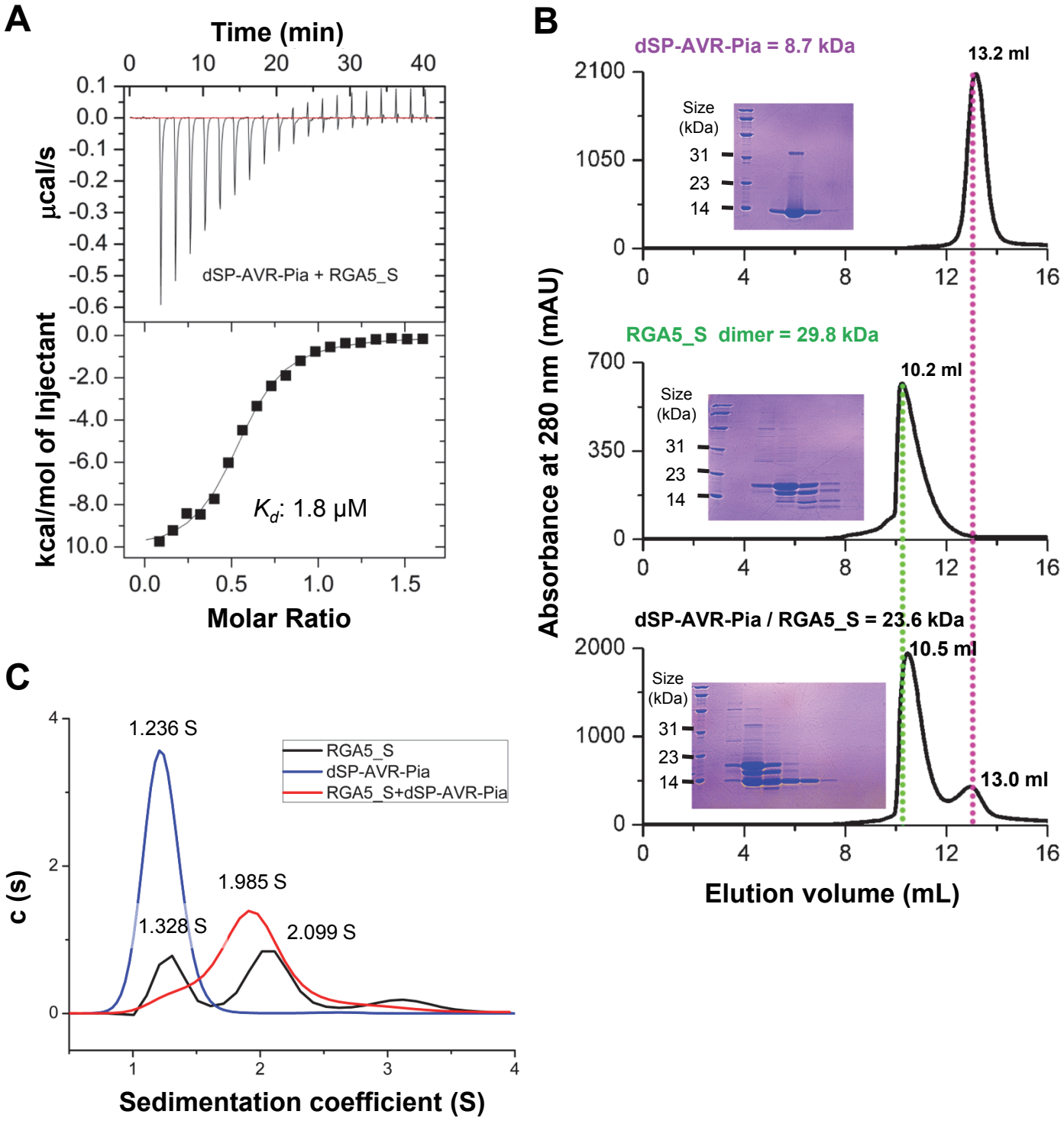

Supplemental Figure 2: dSP-AVR-Pia binds RGA5_S with moderate affinity and competes with RGA5_S self-interaction in RGA5_S/dSP-AVR-Pia complex formation. (A) ITC curves for the titration of RGA5_S by dSP-AVR-Pia. The area of each injection peak corresponds to the total heat released for that injection. The bottom panel shows the integrated heat of injections (squares) and the best fit (solid line) to a single site binding model calculated with MicroCal Origin software (Origin Lab). (B) Analytical Gel Filtration traces showing the retention volume of dSP-AVR-Pia, RGA5_S and a 1:1 mixture of both proteins and SDS-PAGE gels of relevant elution fractions. (C) Sedimentation coefficient distributions calculated from sedimentation velocity analytical ultracentrifugation (SV-AUC) with dSP-AVR-Pia, RGA5_S and a 1:1 mixture of both proteins. These ITC (A), GF (B) and SV-AUC (C) experiments were repeated three times with similar results.

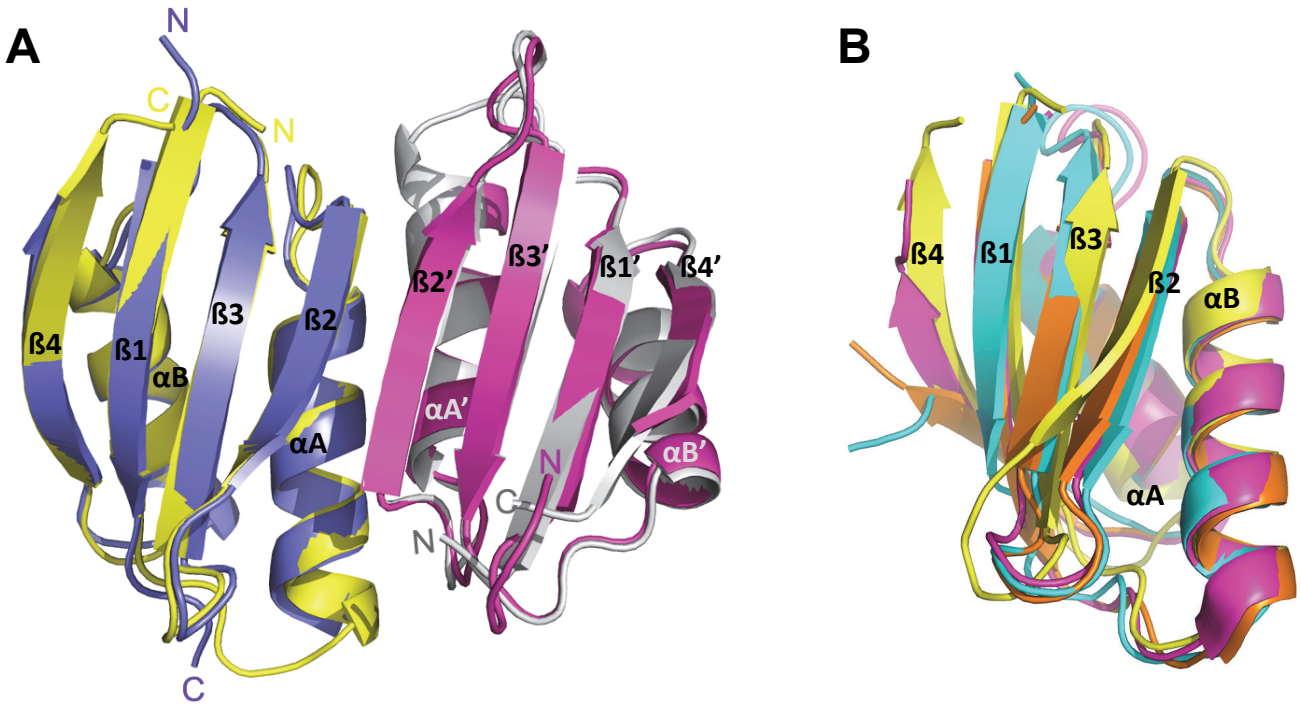

Supplemental Figure 3: $RGA5_{HMA}$ adopts a typical HMA fold and forms homodimers through an interface formed by αA and β2. (A) Overlay of the crystal structures of $RGA5_{HMA}$ (yellow and grey) and $Pikp\text{-}1_{HMA}$ (blue and purple) homodimers. B) Overlay of the crystal structures of HMA domains from different species showing the conservation of the HMA fold. $RGA5_{HMA}$ (yellow), *Cupriavidus metallidurans* (cyan), *Arabidopsis thaliana* (purple), *Synechocystis sp. (strain PCC 6803)* (orange), PDB accession numbers 1OSD, 3DXS and 2XMW.

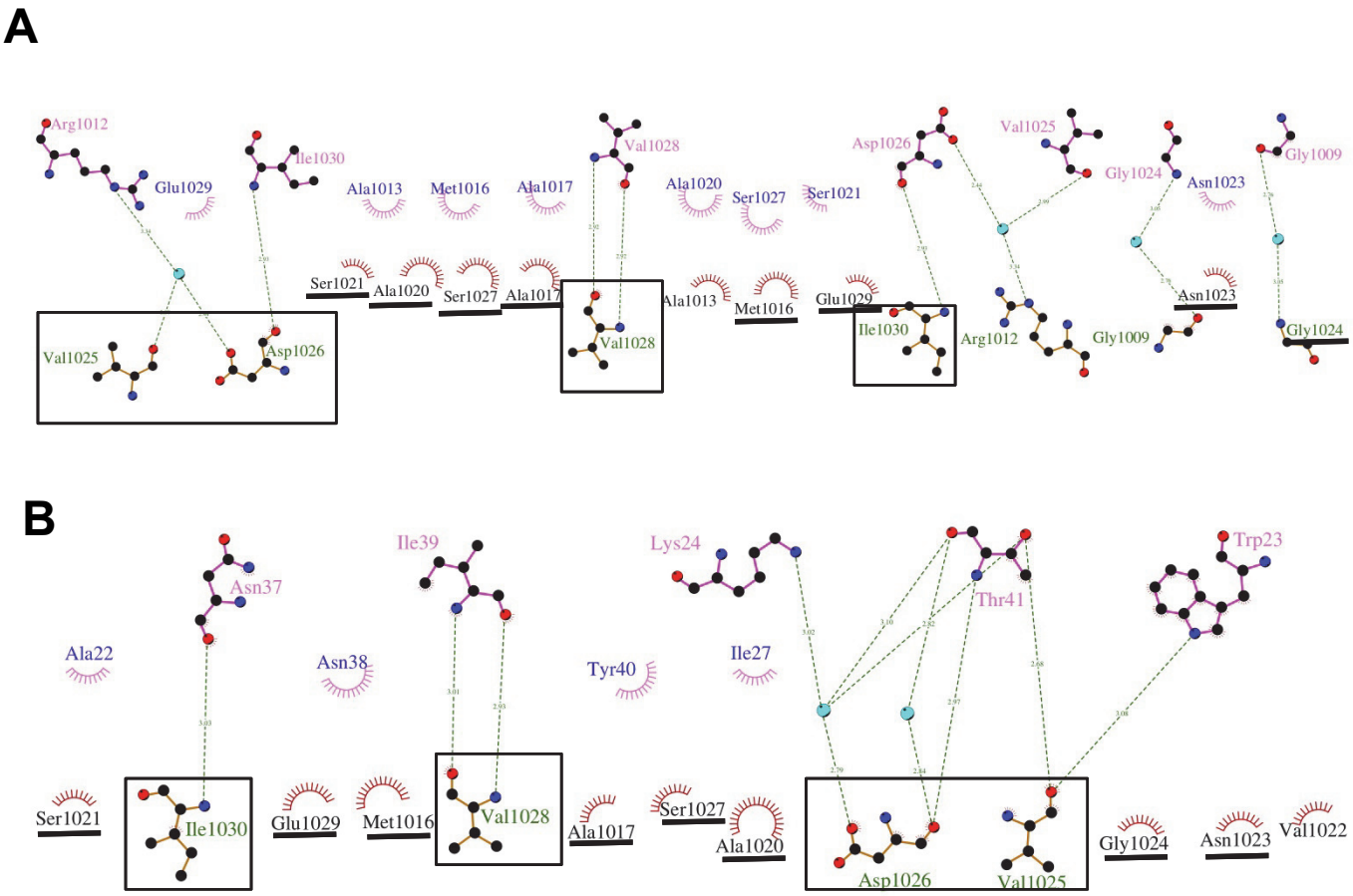

Supplemental Figure 4: Comparison of protein-protein interactions in the RGA5$_{HMA}$ dimer and the RGA5$_{HMA}$/AVR1-CO39 complex. Schematic view (Ligplot v.4.5.3) of inter-residue contacts at the binding interface of the (A) RGA5$_{HMA}$ dimer and the (B) RGA5$_{HMA}$/AVR1-CO39 complex. In (A), interaction contacts are symmetrical and residues are labelled in pink and blue for one monomer and in green and black for the other. In (B), residues of AVR1-CO39 are labelled in pink and blue and residues of RGA5$_{HMA}$ are in green and black. RGA5$_{HMA}$ residues interacting in the homo dimer and in the RGA5$_{HMA}$/AVR1-CO39 complex are highlighted by boxes, if they make hydrogen bonds, and are underlined if they are involved in hydrophobic contacts.

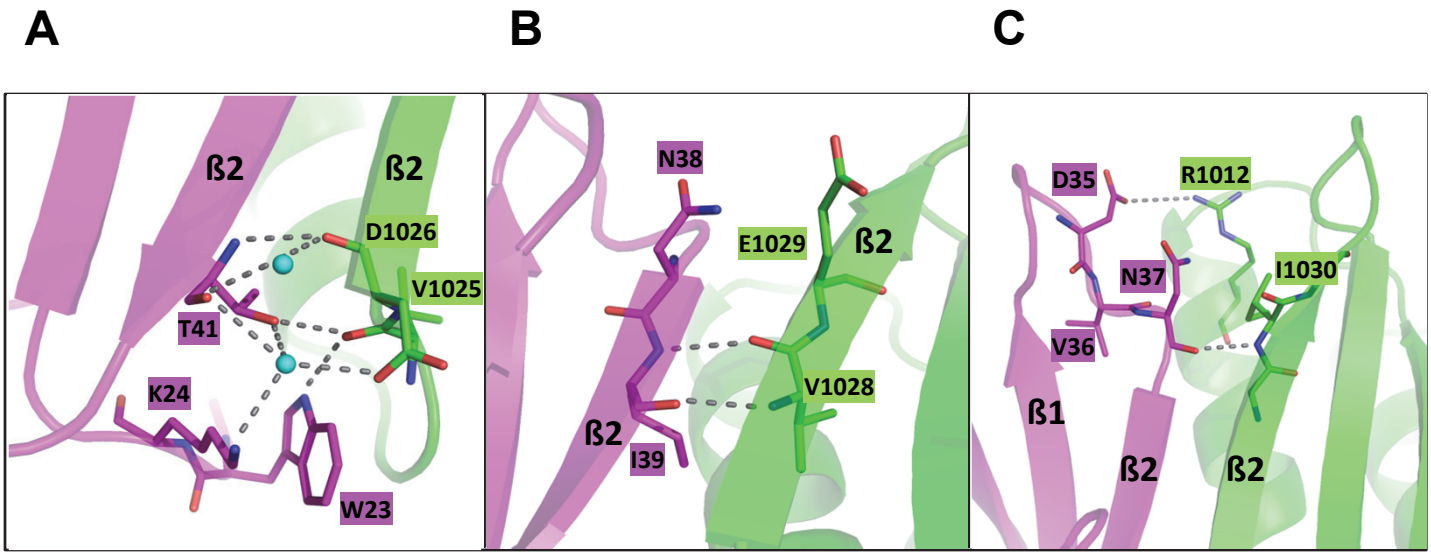

Supplemental Figure 5: Details of the RGA5$_{HMA}$/AVR1-CO39 binding interface. A) The first important area in the RGA5$_{HMA}$/AVR1-CO39 binding interfaces is formed by W23, K24 and T41 in AVR1-CO39 and V1025 and D1026 in RGA5$_{HMA}$. Binding involves main- and side-chain hydrogen bonding between AVR1-CO39^{T41} and RGA5^{D1026}. In addition, the side chain amino group of AVR1-CO39^{K24} forms a water-mediated hydrogen bond with the side chain carboxyl group of RGA5^{D1026}. AVR1-CO39$^{W23:N\varepsilon1}$ and AVR1-CO39$^{T41:O\gamma}$ form hydrogen bonds with the main chain oxygen of RGA5^{V1025}. (B) The second area involves hydrogen bonding between AVR1-CO39^{I39} and RGA5$_{HMA}$^{V1028}. (C) The third interaction site involves a hydrogen bond between the main chain oxygen and nitrogen of AVR1-CO39^{N37} and RGA5^{I1030} respectively. This binding area is further stabilized by stacking interactions of RGA5^{R1012}, with residues in the β1-β2 loop of AVR1-CO39.

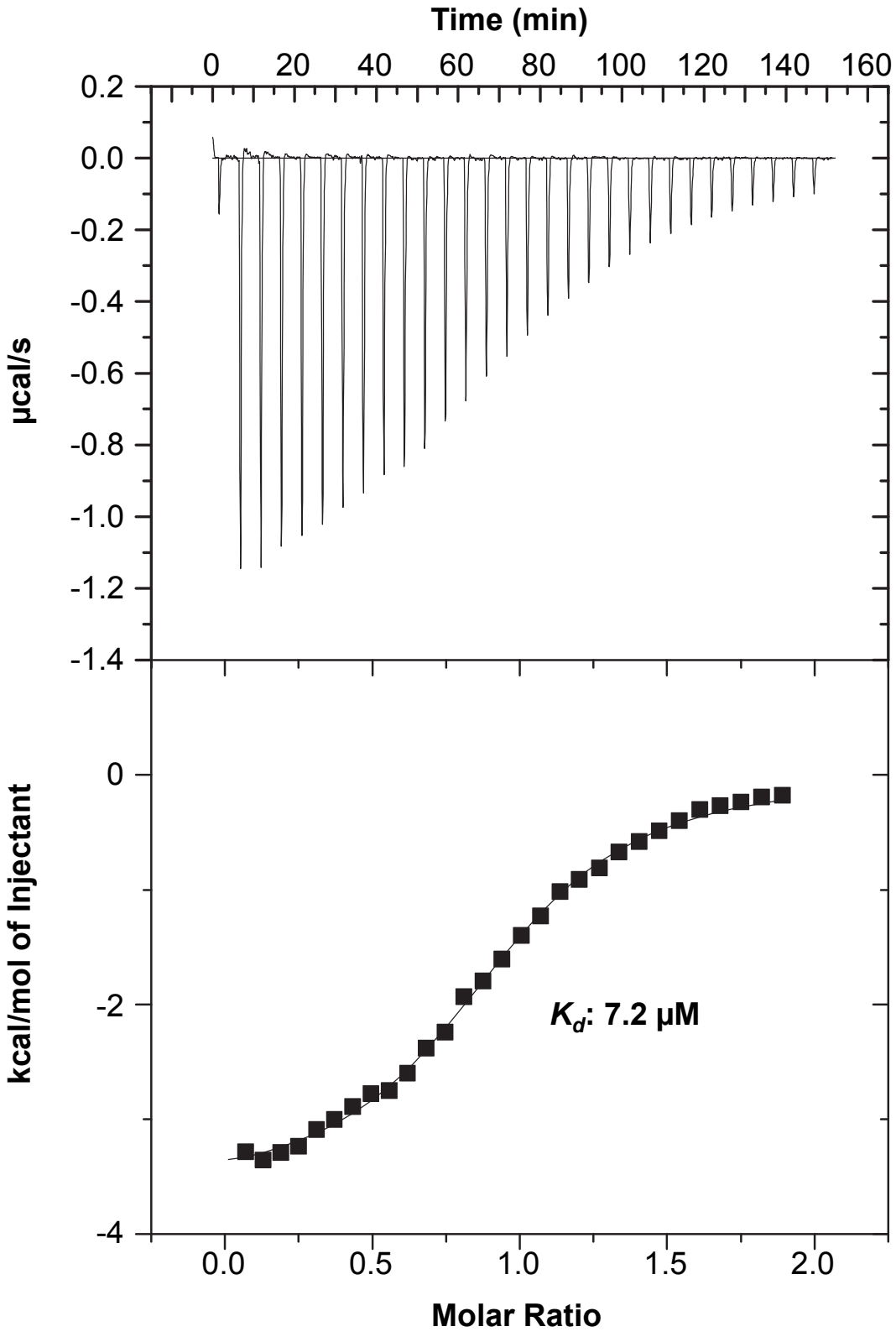

Supplemental Figure 6: The *Kd*s for the $RGA5_{HMA}$/AVR1-CO39 and the RGA5_S/AVR1-CO39 complexes are similar indicating that RGA5_S residues outside the HMA domain do not contribute to AVR1-CO39 binding. ITC curves for the titration of $RGA5_{HMA}$ by dSP-AVR1-CO39. For dSP-AVR1-$CO39^{wt}$ the fit parameters were N=0.938 ±0.00619, K_a=1.39 ± 0.07 10^5 mol^{-1}, ΔH=-3632 ± 33.24 $cal.mol^{-1}$, ΔS= 11.1 $cal.K^{-1}/mol^{-1}$. The experiment was repeated two times with similar results.

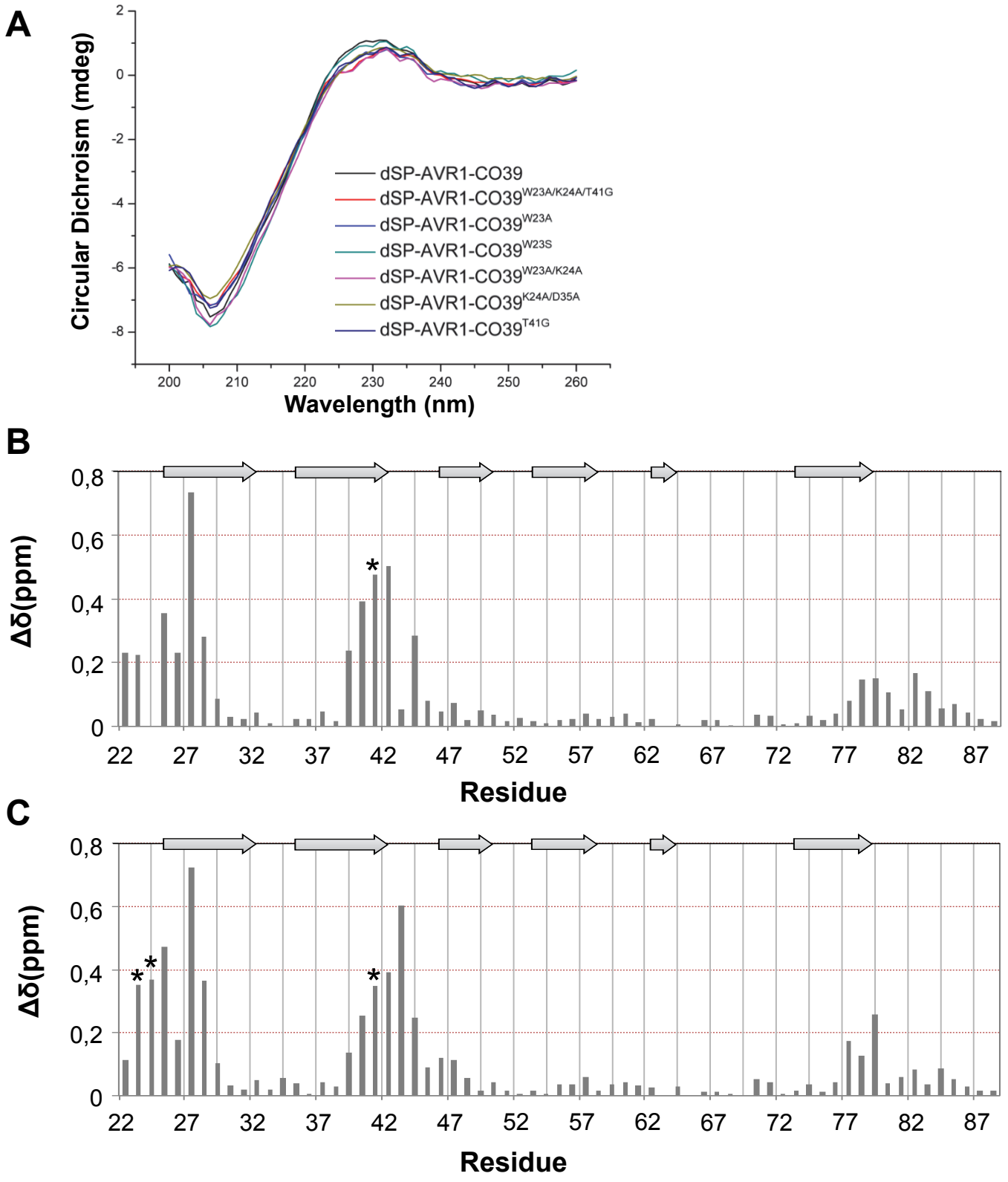

Supplemental Figure 7: Analysis of recombinant proteins of AVR1-CO39 mutants by far-UV circular dichroism (CD) and NMR analysis. (A) AVR1-CO39 wild-type and mutants show almost identical CD spectra indicating that the recombinant proteins are properly folded. (B) Chemical shift differences (Δppm) between dSP-AVR1-CO39 wild-type and dSP-AVR1-CO39^{T41G} and (C) between dSP-AVR1-CO39 wild type and dSP-AVR1-CO39$^{W23A\text{-}K24A\text{-}T41G}$. Chemical shift differences were calculated as the Hamming distance (Schumann et al. 2007), $\Delta\delta(ppm)=I\Delta\delta(^{1}H)_{ij}I + 0.102 \times I\Delta\delta(^{15}N)_{ij}I$, where $\Delta\delta(^{1}H)_{ij}$ and $\Delta\delta(^{15}N)_{ij}$ are the chemical shift differences observed between the wild-type protein and each mutant. The asterisks show mutated residues.

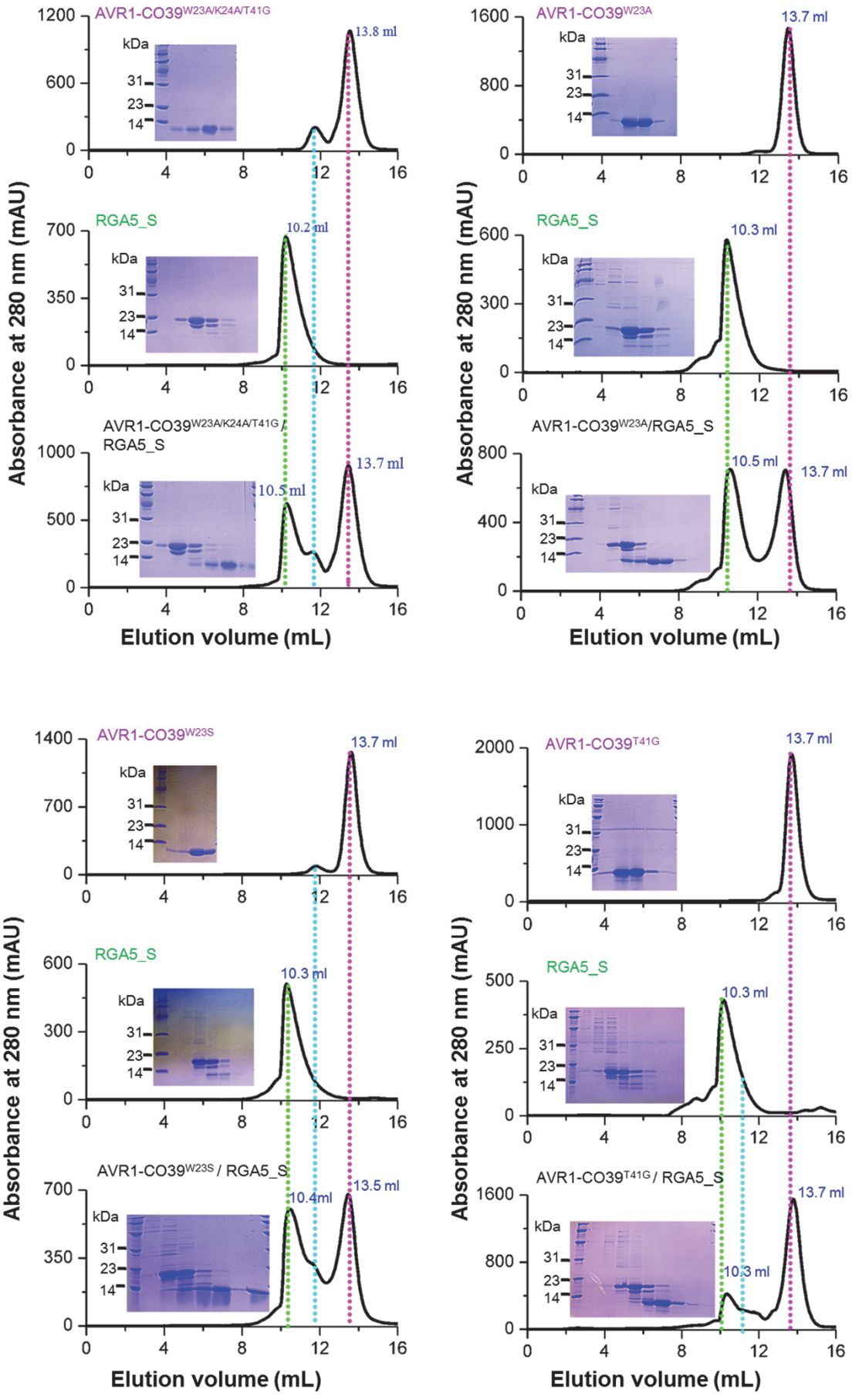

Supplemental Figure 8: Gel filtration assays demonstrate the importance of binding area 1 in the HMA-binding interface of AVR1-CO39 for RGA5_S/dSP-AVR1-CO39 complex formation. Gel Filtration traces showing the retention volume and SDS-PAGE gels of relevant elution fractions of dSP-AVR1-CO39 mutants, RGA5_S and 1:1 mixtures of both proteins. The figure shows representative results of three consistent experimental repeats.

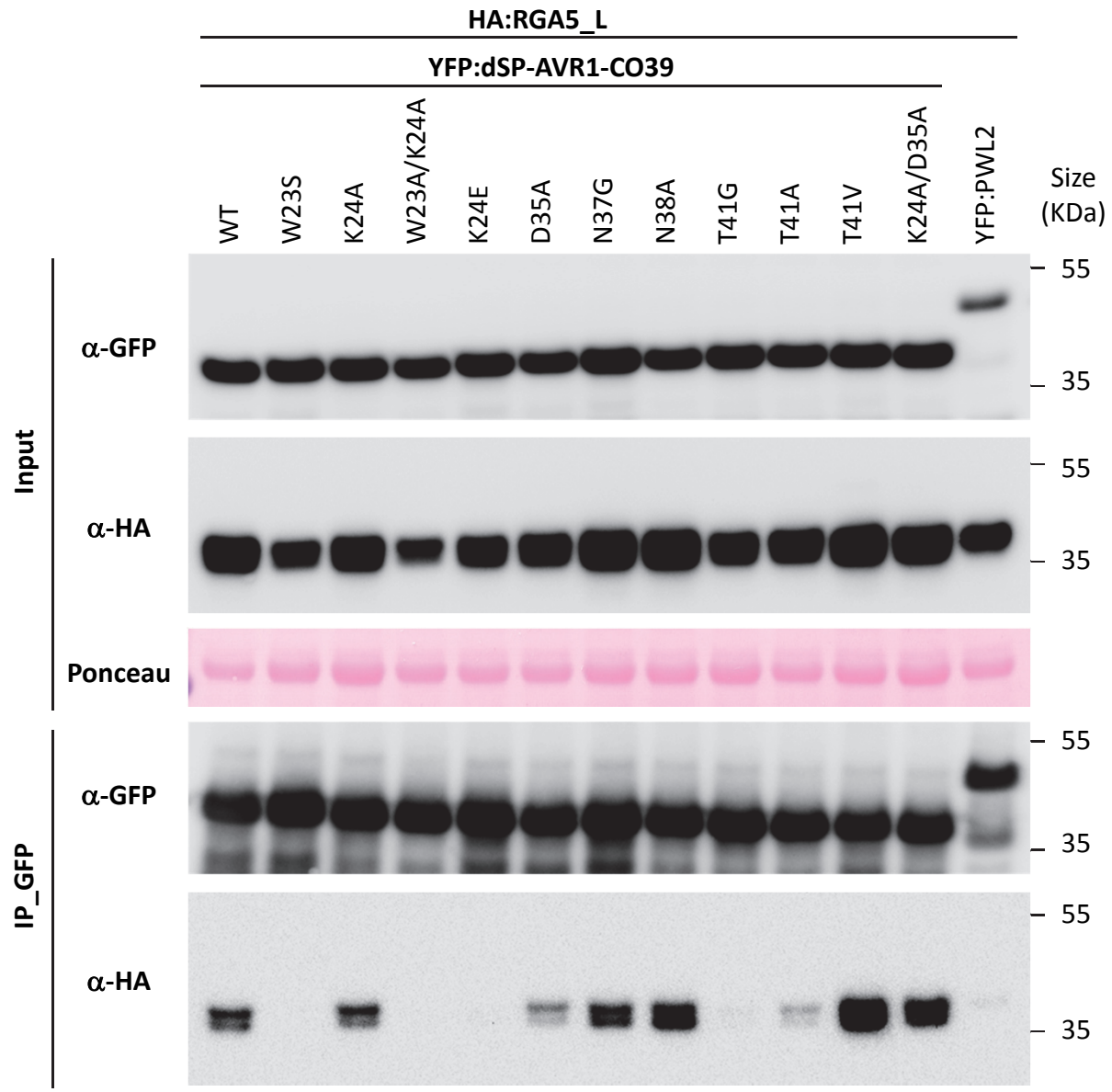

Supplemental Figure 9: Key residues within the HMA-binding surface of AVR1-CO39 are required for *in planta* association with RGA5_L. HA:RGA5_L was co-expressed in *N. benthamiana* leaves with YFP-fused wild type dSP-AVR1-CO39 (WT) or dSP-AVR1-CO39 variants carrying point mutations in the HMA-binding surface. Tagged proteins were detected in the extract (input) and after immunoprecipitation with anti-GFP beads (IP-GFP) by immunoblotting with anti-HA (α-HA) and anti-GFP (α-GFP) antibodies. The *M. oryzae* effector PWL2 was used as a control for specificity. Protein loading in the input is shown by Ponceau staining. The experiment has been performed twice with consistent results.

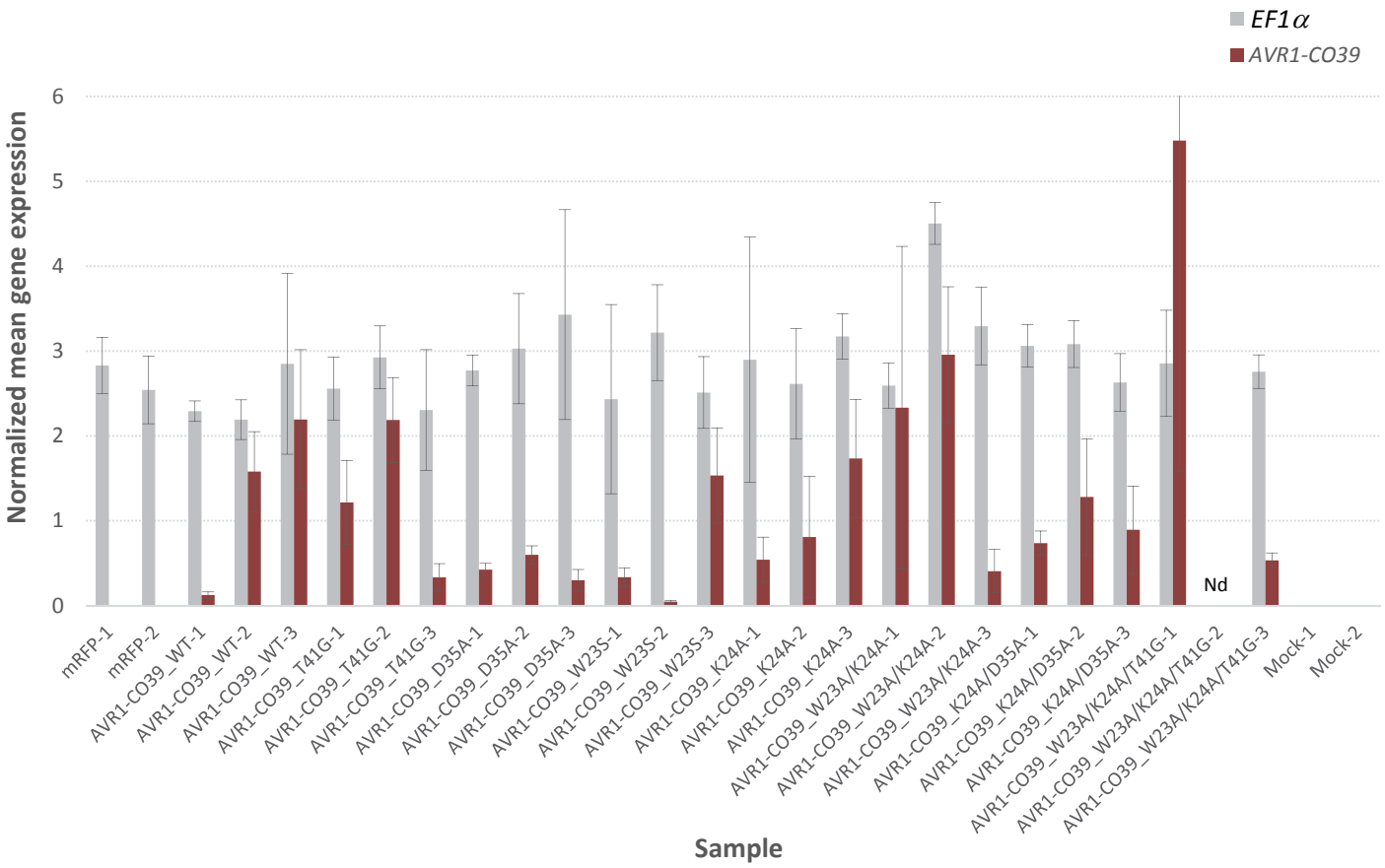

Supplemental Figure 11: *AVR1-CO39* mutants are properly expressed during plant infection. mRNA levels of *AVR1-CO39* and the constitutively expressed genes *elongation factor 1α* (*EF1α* , *MGG_03641*) and *actin* (*MGG_03982*) were determined for the different transgenic *M. oryzae* isolates by qRT-PCR using leaf samples of the susceptible rice variety Nipponbare harvested 4 days after *M. oryzae* infection. Relative expression levels were calculated by using expression of constitutively expressed *actin* (*MGG_03982*) as a reference. Mean values and standard deviations were calculated from four independent biological samples. Nd: non determined.

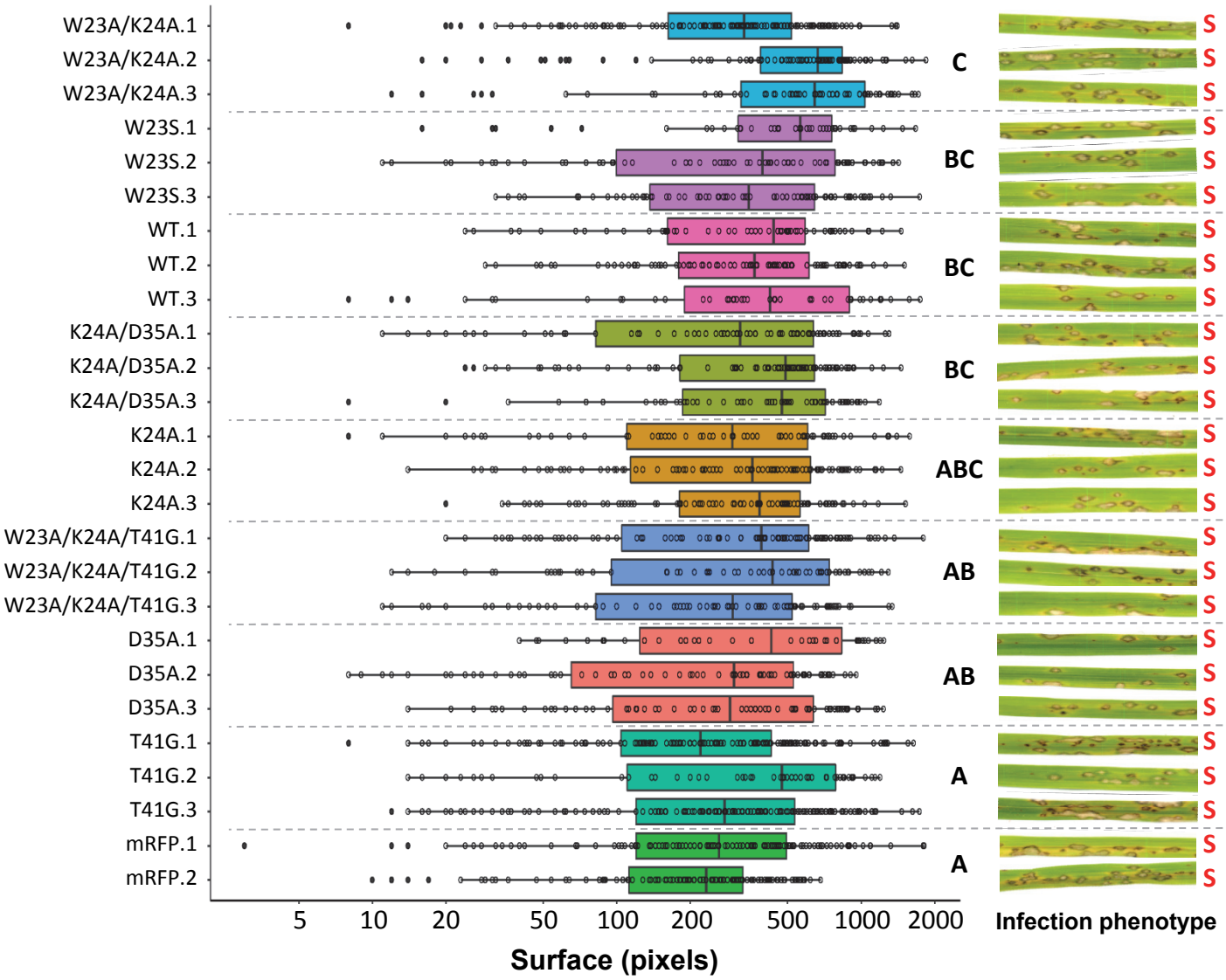

Supplemental Figure 10: Mutations of key residues within the HMA-binding surface of AVR1-CO39 do not impair fungal virulence. Transgenic *M. oryzae* isolates carrying wild type *AVR1-CO39* (WT), *AVR1-CO39* variants affected in the HMA-binding surface or the *mRFP* (control), were spray inoculated on 3-week-old plants of the rice cultivar Nipponbare (NB) that lacks the *Pi-CO39* resistance. Three independent transgenic isolates were generated for each construct with the exception of the mRFP construct for which two isolates were tested. Leaves from 10 different plants for each isolate tested were scanned 7 days after inoculation and lesions areas were measured and plotted. The boxes represent the first quartile, median, and third quartile. To determine whether lesion areas induced by the different AVR1-CO39 mutants on rice are significantly different, a log-transformation was applied to the data prior to an ANOVA followed by a Tukey HSD test. Groups with the same letter (A to C) are not significantly different at level 0.05. Representative disease phenotypes are shown (right panel) for each strain (S: susceptible, I: intermediate, R: resistant).

Table 1. X-ray data collection and refinement statistics.

	RGA5_S	RGA5_S/dSP-AVR1-CO39
Wavelength (Å)	0.9795	0.9795
Resolution range (Å) [a]	39.33-1.78 (1.84-1.78)	27.92-2.19 (2.27-2.19)
Space group	$P4_322$	$P3_121$
Unit cell		
a, b, c (Å)	55.62, 55.62, 78.33	66.72, 66.72, 108.33
α, β, γ (°)	90, 90, 90	90, 90, 120
Total reflections	301966 (31225)	253846 9579)
Unique reflections	12343 (1194)	14412 (1198)
Multiplicity	24.5 (26.2)	17.6 (8.0)
Completeness (%)	96.9 (98.9)	96.59 (81.28)
Mean I/sigma (I)	29.45 (2.66)	29.37 (2.69)
Wilson B-factor (Å^2)	29.9	50.13
R-merge	0.07 (1.74)	0.06 (0.768)
R-meas	0.07 (1.77)	0.07 (0.82)
R-pim	0.01 (0.34)	0.02(0.28)
$CC_{1/2}$	1 (0.955)	1 (0.794)
CC*	1 (0.988)	1 (0.941)
Reflections used in refinement	11896 (1181)	14409 (1198)
Reflections used for R-free	616 (65)	686 (37)
R-work	0.218 (0.339)	0.162 (0.271)
R-free	0.238 (0.365)	0.197(0.288)
CC(work)	0.952 (0.903)	0.972 (0.810)
CC(free)	0.922 (0.817)	0.964 (0.759)
Number of non-hydrogen atoms	594	1123
- macromolecules	553	1086
- solvent	41	37
Protein residues	73	141
RMS(bonds) (Å)	0.006	0.008
RMS(angles) (°)	0.81	1.24
Ramachandran favored (%)	98.59	96.35
Ramachandran allowed (%)	1.41	3.65
Ramachandran outliers (%)	0.00	0.00
Rotamer outliers (%)	0.00	0.00
Molprobity clashscore	2.58	2.73
Molprobity overall score	1.04	1.30
Average B-factor (Å^2)	44.25	65.65
macromolecules	43.62	65.80
solvent	53.44	61.32
Number of TLS groups	6	11

[a]: Values in parentheses denote the highest resolution shell.

phenix.table_one has been used to calculated the table.

$R_{merge} = 100 \times \Sigma_{hkl} \Sigma_i |I_i(hkl) - \langle I(hkl) \rangle| / \Sigma_{hkl} \Sigma_i I_i(hkl)$, where $\langle I(hkl) \rangle$ is the mean value of $I(hkl)$.

$R_{work} = 100 \times \Sigma_{hkl} ||F_o| - |F_c|| / \Sigma_{hkl} |F_o|$, where F_o and F_c the observed and calculated structure factors, respectively.

R_{free} is calculated as for R_{work}, but for the test set comprising 5% reflections not used in refinement.

Table S2

Primers	Sequence
oCS087	GGGGACAAGTTTGTACAAAAAAGCAGGCTTAGCTTGGAAAGATTGCATCATCCAA
oCS088	GGGGACCACTTTGTACAAGAAAGCTGGGTCTCAACAAGACTCATCGTCGTCAGC
oCS346	GGGGACAAGTTTGTACAAAAAAGCAGGCTTACTCAGAAAAACAGGGCTAAAGCAAAA
oCS347	GGGGACCACTTTGTACAAGAAAGCTGGGTCTCAATCTTTATTTGCTTGGCTGACCTGC
oCS387	CAAAAAAGCAGGCTTAGCTTCGAAAGATTGCATCATCCAAC
oCS388	GTTGGATGATGCAATCTTTCGAAGCTAAGCCTGCTTTTTTG
oCS389	CAAAAAAGCAGGCTTAGCTTGGGCAGATTGCATCATCCAACGTTAT
oCS390	ATAACGTTGGATGATGCAATCTGCCCAAGCTAAGCCTGCTTTTTTG
oCS391	CCAACTTTGTACAAAAAAGCAGGCTTAGCTGCGGCAGATTGCATCATCCAACGTTATAAAG
oCS392	CTTTATAACGTTGGATGATGCAATCTGCCGCAGCTAAGCCTGCTTTTTTGTACAAAGTTGG
oCS393	CAAAAAAGCAGGCTTAGCTTGGGAGGATTGCATCATCCAACGTTATA
oCS394	TATAACGTTGGATGATGCAATCCTCCCAAGCTAAGCCTGCTTTTTTG
oCS395	CCAACGTTATAAAGACGGCGCTGTCAACAACATATATACTG
oCS396	CAGTATATATGTTGTTGACAGCGCCGTCTTTATAACGTTGG
oCS397	CCTATTGGCAGTATATATGTTGCCGACATCGCCGTCTTTATAACGT
oCS398	ACGTTATAAAGACGGCGATGTCGGCAACATATATACTGCCAATAGG
oCS399	GTTATAAAGACGGCGATGTCAACGCCATATATACTGCCAATAGGAACG
oCS400	CGTTCCTATTGGCAGTATATATGGCGTTGACATCGCCGTCTTTATAAC
oCS401	AAAGACGGCGATGTCAACAACATATATGGTGCCAATAGGAACG
oCS402	CGTTCCTATTGGCACCATATATGTTGTTGACATCGCCGTCTTT
oCS403	TTCCTATTGGCAGCATATATGTTGTTGACATCGCCGTC
oCS404	GACGGCGATGTCAACAACATATATGCTGCCAATAGGAA
oCS405	CGTTATAAAGACGGCGATGTCAACAACATATATGTTGCCAATAGGAACGAAG
oCS406	CTTCGTTCCTATTGGCAACATATATGTTGTTGACATCGCCGTCTTTATAACG
oCS407	GCAGGCTTAGCTTGGGCAGATTGCATCATCCAACGTTATAAAGACGGCGCTGTCAACAACATATATACTGC
oCS408	GCAGTATATATGTTGTTGACAGCGCCGTCTTTATAACGTTGGATGATGCAATCTGCCCAAGCTAAGCCTGC
oCS411	TCCAGCAGCCAATGCTTCGAAAGATTGCATCATCC
oCS412	GGATGATGCAATCTTTCGAAGCATTGGCTGCTGGA
oCS413	CCAGCAGCCAATGCTTGGGCAGATTGCATCATCCAACG
oCS414	CGTTGGATGATGCAATCTGCCCAAGCATTGGCTGCTGG
oCS415	GGCTTACTTTCCAGCAGCCAATGCTGCGGCAGATTGCATCATCCAACGTTA
oCS416	TAACGTTGGATGATGCAATCTGCCGCAGCATTGGCTGCTGGAAAGTAAGCC
Actin_f	TCTTCGAGACCTTCAACGCC
Actin_r	ACCGGAGTCGAGCACGATAC
EF1_f	GCCCGGTATGGTCGTTACCT
EF1_r	AGCTGCTGGTGGTGCATCTC
AVR1-CO39_f	CTGCCATCCCTACCCAGTTA
AVR1-CO39_r	GACTCATCGTCGTCAGCGTA

Table S3

Use	Final plasmid	Cloning Method	Template	Cloning primers	Backbone vector	Insert	Reference
Entry vectors for LR cloning	pSC046	GTW BP	pSC001	oCS087/oCS088	pDONR207	dSP-AVR1-CO39 with stop	(Cesari et al. 2013)
	pSC563	quikchange	pSC046	oCS387/oCS388	pDONR207	dSP-AVR1-CO39 W2S with stop	
	pSC564	quikchange	pSC046	oCS389/oCS390	pDONR207	dSP-AVR1-CO39 K3A with stop	
	pSC565	quikchange	pSC046	oCS391/oCS392	pDONR207	dSP-AVR1-CO39 W2A K3A with stop	
	pSC566	quikchange	pSC046	oCS393/oCS394	pDONR207	dSP-AVR1-CO39 K3E with stop	
	pSC567	quikchange	pSC046	oCS395/oCS396	pDONR207	dSP-AVR1-CO39 D14A with stop	
	pSC568	quikchange	pSC046	oCS397/oCS398	pDONR207	dSP-AVR1-CO39 N16G with stop	
	pSC569	quikchange	pSC046	oCS399/oCS400	pDONR207	dSP-AVR1-CO39 N17A with stop	
	pSC570	quikchange	pSC046	oCS401/oCS402	pDONR207	dSP-AVR1-CO39 T20G with stop	
	pSC571	quikchange	pSC046	oCS403/oCS404	pDONR207	dSP-AVR1-CO39 T20A with stop	
	pSC572	quikchange	pSC046	oCS405/oCS406	pDONR207	dSP-AVR1-CO39 T20V with stop	
	pSC573	quikchange	pSC046	oCS407/oCS408	pDONR207	dSP-AVR1-CO39 K3A D14A with stop	
	pSC129	/	/	/	pDONR207	RGA5_L with stop	Cesari et al. 2013
	pSC500	GTW BP	pSC496	oCS346/oCS347	pDONR207	Pikp-1_HMA with stop	
Y2H	pSC575	GTW LR	pSC563	/	pGBKT7-GW	BD:dSP-AVR1-CO39 W2S	
	pSC576	GTW LR	pSC564	/	pGBKT7-GW	BD:dSP-AVR1-CO39 K3A	
	pSC577	GTW LR	pSC565	/	pGBKT7-GW	BD:dSP-AVR1-CO39 W2A K3A	
	pSC578	GTW LR	pSC566	/	pGBKT7-GW	BD:dSP-AVR1-CO39 K3E	
	pSC579	GTW LR	pSC567	/	pGBKT7-GW	BD:dSP-AVR1-CO39 D14A	
	pSC580	GTW LR	pSC568	/	pGBKT7-GW	BD:dSP-AVR1-CO39 N16G	
	pSC581	GTW LR	pSC569	/	pGBKT7-GW	BD:dSP-AVR1-CO39 N17A	
	pSC582	GTW LR	pSC570	/	pGBKT7-GW	BD:dSP-AVR1-CO39 T20G	
	pSC583	GTW LR	pSC571	/	pGBKT7-GW	BD:dSP-AVR1-CO39 T20A	
	pSC584	GTW LR	pSC572	/	pGBKT7-GW	BD:dSP-AVR1-CO39 T20V	
	pSC585	GTW LR	pSC573	/	pGBKT7-GW	BD:dSP-AVR1-CO39 K3A D14A	
	pSC600	GTW LR	pSC046	/	pGBKT7-GW	BD:AVR1-CO39	
	pSC547	GTW LR	pSC500	/	pGADT7-GW	AD:HMA Pikp1 bornes TS + stop	
	pCV226	GTW LR	pSC129	/	pGADT7-GW	AD:RGA5-L	
Co-IP	pSC586	GTW LR	pSC563	/	pBIN19-P35S-YFP-GTW	YFP:dSP-AVR1-CO39 W2S	
	pSC587	GTW LR	pSC564	/	pBIN19-P35S-YFP-GTW	YFP:dSP-AVR1-CO39 K3A	
	pSC588	GTW LR	pSC565	/	pBIN19-P35S-YFP-GTW	YFP:dSP-AVR1-CO39 W2A K3A	
	pSC589	GTW LR	pSC566	/	pBIN19-P35S-YFP-GTW	YFP:dSP-AVR1-CO39 K3E	
	pSC590	GTW LR	pSC567	/	pBIN19-P35S-YFP-GTW	YFP:dSP-AVR1-CO39 D14A	
	pSC591	GTW LR	pSC568	/	pBIN19-P35S-YFP-GTW	YFP:dSP-AVR1-CO39 N16G	
	pSC592	GTW LR	pSC569	/	pBIN19-P35S-YFP-GTW	YFP:dSP-AVR1-CO39 N17A	
	pSC593	GTW LR	pSC570	/	pBIN19-P35S-YFP-GTW	YFP:dSP-AVR1-CO39 T20G	
	pSC594	GTW LR	pSC571	/	pBIN19-P35S-YFP-GTW	YFP:dSP-AVR1-CO39 T20A	
	pSC595	GTW LR	pSC572	/	pBIN19-P35S-YFP-GTW	YFP:dSP-AVR1-CO39 T20V	
	pSC596	GTW LR	pSC573	/	pBIN19-P35S-YFP-GTW	YFP:dSP-AVR1-CO39 K3A D14A	
	pSC079	GTW LR	pSC046	/	pBIN19-P35S-YFP-GTW	YFP-dSP-AvrCO39	
	pDO119	/	/	/	pBIN19-P35S-YFP-GTW	YFP:PWL2	Ortiz et al. 2017
	pSC144	GTW LR	pSC129		pBIN19-P35S-3HA-GTW	3HA:RGA5_L	
***Magnaporthe oryzae* transformation**	pCV10	yeast gap repair	genomic DNA of *M. oryzae* IN03	oTK017_c/oTK036	pDL02	pRP27::SP-AVR1-CO39 WT	identical to pCB027 from Ribot et al, 2013
	pSC619	quikchange	pCV010	oCS401/oCS402	pDL02	pRP27::SP-AVR1-CO39 T20G	
	pSC620	quikchange	pCV010	oCS395/oCS396	pDL02	pRP27::SP-AVR1-CO39 D14A	
	pSC621	quikchange	pCV010	oCS411/oCS412	pDL02	pRP27::SP-AVR1-CO39 W2S	
	pSC622	quikchange	pCV010	oCS413/oCS414	pDL02	pRP27::SP-AVR1-CO39 K3A	
	pSC623	quikchange	pCV010	oCS415/oCS416	pDL02	pRP27::SP-AVR1-CO39 W2A K3A	
	pSC624	quikchange	pSC620	oCS413/oCS414	pDL02	pRP27::SP-AVR1-CO39 K3A D14A	
	pSC625	quikchange	pSC619	oCS415/oCS416	pDL02	pRP27::SP-AVR1-CO39 W2A K3A T20G	
	pCR17	/	/	/	pDL02	pRP27::mRFP	Ribot et al., 2013
Other vectors	pSC496	/	/	/	pCambia1300	Pikp-1 full lenght	Maqbool et al. 2015
	pDL02	/	/	/	/	/	Bruno *et al* , 2004
	pGADT7-GW	/	/	/	/	/	Bernoux et al., 2011
	pGBKT7-GW	/	/	/	/	/	Bernoux et al., 2011

Supplementary references

1. Guo L, et al. (2018) Crystallization of the rice immune receptor RGA5A_S with the rice blast fungus effector AVR1□CO39 prepared via mixture and tandem strategies. *Acta Crystallogr F Struct Biol Commun* F47:262–267.

2. de Guillen K, et al. (2015) Structure analysis uncovers a highly diverse but structurally conserved effector family in phytopathogenic fungi. *PLoS Pathog* 11(10):e1005228.

3. Ortiz D, et al. (2017) Recognition of the Magnaporthe oryzae effector AVR-Pia by the decoy domain of the rice NLR immune receptor RGA5. *Plant Cell* 29(1):156–168.

4. Studier FW (2005) Protein production by auto-induction in high density shaking cultures. *Protein Expr Purif* 41(1):207–234.

5. Winn MD, et al. (2011) Overview of the CCP 4 suite and current developments research papers. *Acta Crystallogr D Biol Crystallogr* D4449:235–242.

6. Winter G (2010) xia2: an expert system for macromolecular crystallography data reduction. *J Appl Crystallogr* 43(1):186–190.

7. McCoy AJ, et al. (2007) Phaser crystallographic software. *J Appl Crystallogr* 40(4):658–674.

8. Emsley P, et al. (2010) Features and development of Coot. *Acta Crystallogr D Biol Crystallogr* D66:486–501.

9. Chen VB, et al. (2010) MolProbity : all-atom structure validation for macromolecular crystallography. *Acta Crystallogr D Biol Crystallogr* D66:12–21.

10. Wishart DS, et al. (1995) 1H, 13C and 15N chemical shift referencing in biomolecular NMR. *J Biomol NMR* 6(2):135–140.

11. Vranken WF, et al. (2005) The CCPN data model for NMR spectroscopy: Development of a software pipeline. *Proteins Struct Funct Bioinforma* 59(4):687–696.

12. Schumann FH, et al. (2007) Combined chemical shift changes and amino acid specific chemical shift mapping of protein-protein interactions. *J Biomol NMR* 39(4):275–289.

13. Brown PH, Schuck P (2006) Macromolecular size-and-shape distributions by sedimentation velocity analytical ultracentrifugation. *Biophys J* 90:4651–4661.

14. Faivre-Rampant O, et al. (2008) Characterization of the model system rice-Magnaporthe for the study of nonhost resistance in cereals. *New Phytol* 180(4):899–910.

15. Cesari S, et al. (2013) The rice resistance protein pair RGA4/RGA5 recognizes the Magnaporthe oryzae effectors AVR-Pia and AVR1-CO39 by direct binding. *Plant Cell* 25(4):1463–81.

16. Kushnirov V V. (2000) Rapid and reliable protein extraction from yeast. *Yeast* 16(9):857–860.